

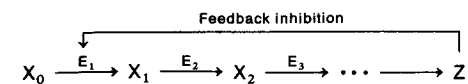
## Regulation of biological activity

## 17-1 BIOLOGICAL REGULATION

In Chapters 15 and 16, we discussed equilibrium and kinetic features of ligand interactions with macromolecules. Our emphasis was placed on general features, with the idea of developing insight into basic principles. In this chapter we direct attention to special properties associated with the regulation of biological activity, and to two prominent examples: aspartate transcarbamoylase and hemoglobin. These two well-studied systems beautifully illustrate how multiple-ligand interactions modulate biological activity. In addition, they provide good illustrations and tests of theories that have been developed to explain regulation of the biological activity of a protein.

## Feedback Inhibition

A good example of biological regulation is the phenomenon of *feedback inhibition*. Consider a pathway in which precursor  $X_0$  is converted by a series of reactions to compound  $Z$ , with each step in the pathway catalyzed by a specific enzyme  $E_i$ . In many cases it is found that, no matter how much  $X_0$  is supplied, the system does not continuously produce a corresponding amount of  $Z$  unless  $Z$  is drained off as it is made. This situation arises because  $Z$  itself feedback-inhibits the enzyme ( $E_1$ ) that converts  $X_0$  to the next compound ( $X_1$ ) on the pathway to  $Z$ :



(17-1)

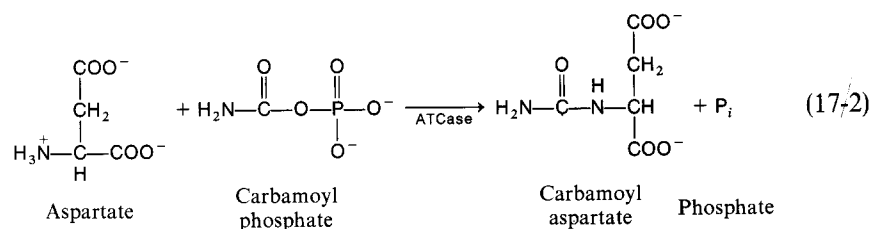
As the concentration of  $Z$  rises, it eventually becomes sufficiently high to inhibit  $E_1$ . In this way,  $Z$  regulates its own synthesis. The inhibition is reversible, so that a decrease in ( $Z$ ) removes the inhibition on  $E_1$  and allows new synthesis of  $Z$ . Note that the cell efficiently avoids the needless expenditure of metabolic energy by having  $Z$  act on the first enzyme in the pathway (rather than on a later one).

In most cases, the end product  $Z$  is structurally unrelated to  $X$ . Therefore,  $Z$  is not a competitive inhibitor of  $E_1$ ; rather  $E_1$  has a special, separate site that is specifically designed to accommodate  $Z$ .

An example of the foregoing is provided by the biosynthesis of nucleic acids. In cells that are rapidly dividing and growing, nucleic acids are continuously synthesized through a general pathway of precursors  $\rightarrow \dots \rightarrow$  nucleotides  $\rightarrow \dots \rightarrow$  nucleic acids. However, if for some reason nucleic acid synthesis slows down, nucleotides do not indefinitely accumulate, even though precursors are available. That is, slowing down the conversion of nucleotides to nucleic acids also inhibits the production of nucleotides.

### The pyrimidine pathway and aspartate transcarbamoylase

A well-studied example of feedback inhibition is from the pyrimidine pathway, in which the first step is catalyzed by aspartate transcarbamoylase (ATCase). The reaction catalyzed by ATCase is



In this reaction, aspartate and carbamoyl phosphate are condensed to give carbamoyl aspartate. After this, there are several steps by which carbamoyl aspartate is converted into the pyrimidine nucleoside triphosphate UTP and, subsequently, to CTP. The end product CTP in turn feedback-inhibits ATCase.

### Allosteric proteins

ATCase is known as an allosteric protein ("allo-" means "other"), a name commonly assigned to proteins that have sites (regulatory sites) specific for physiological molecules that regulate the protein's activity; these sites are other than and distinct from the catalytic site. Allosteric proteins have a number of unusual features, which we shall illustrate and subsequently analyze in quantitative terms. Because it is such a

well-studied system, we use ATCase as an example. However, the concepts discussed are not limited simply to this particular system.

## 17-2 SOME FEATURES AND PROPERTIES OF ALLOSTERIC ENZYMES

### Sigmoidal curves

A striking feature of allosteric enzymes is that they commonly display nonhyperbolic kinetics. Figure 17-1 compares the profiles of initial reaction velocity,  $v_i$ , versus substrate concentration, ( $S$ ), for a "normal" and an allosteric enzyme. A sigmoidal

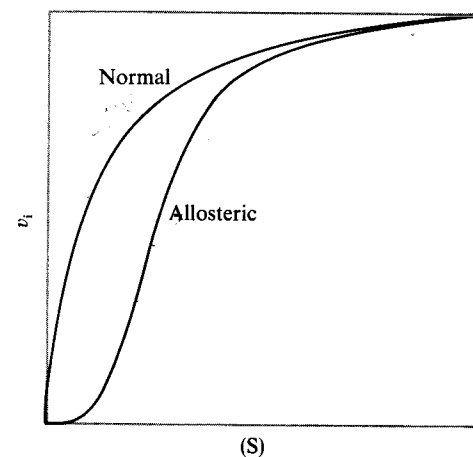


**Figure 17-1**

*Hyperbolic and sigmoidal reaction kinetics.* In a plot of initial reaction velocity  $v_i$  versus substrate concentration ( $S$ ), a "normal" enzyme shows a hyperbolic curve, whereas an allosteric enzyme shows a sigmoidal curve.

curve is observed for the allosteric enzyme. At low substrate concentrations, the velocity is weakly responsive to increases in concentration. As substrate concentration is raised, however, a point is reached at which the velocity steeply rises in response to small increases in substrate concentration; that is, cooperative behavior is exhibited. This kind of kinetic behavior is in sharp contrast to the hyperbolic Michaelis-Menten behavior of the normal enzyme.

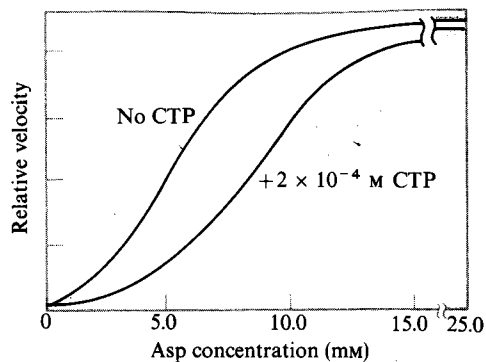
In the appropriate concentration range, the sigmoidal curve of  $v_i$  versus ( $S$ ) enables the enzyme to produce sharp changes in the rate of product formation in response to small variations in substrate concentration.

### Effect of an allosteric inhibitor

Figure 17-2 illustrates the effect of an allosteric inhibitor—CTP in the case of ATCase—on the  $v_i$  versus ( $S$ ) curve. In this example, the inhibitor (CTP) shifts the

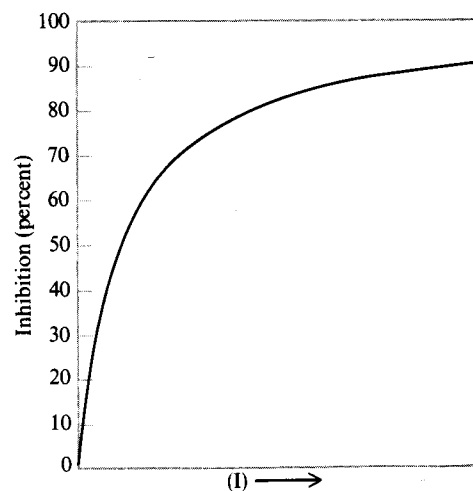
**Figure 17-2**

Effect of an allosteric inhibitor. Relative reaction velocity is plotted against substrate (aspartate) concentration for ATCase in the presence and absence of the allosteric inhibitor CTP. [After J. C. Gerhart and A. B. Pardee, *Cold Spring Harbor Symp. Quant. Biol.* 28:491 (1963).]

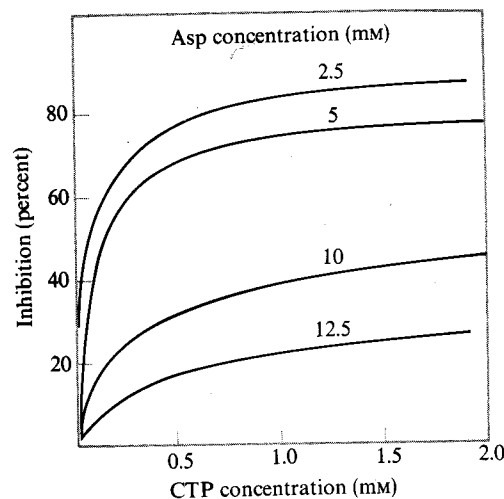


sigmoidal curve to the right, so that higher concentrations of substrate (Asp) are required to achieve the same velocity as in the absence of CTP. At sufficiently high (S), the effect of the inhibitor is overcome. Because high (S) can overcome the inhibition, the situation appears superficially similar to simple competitive inhibition.

However, in the case of ATCase, there is a feature critical to the inhibition that clearly distinguishes it from simple competitive inhibition. We now plot percentage of inhibition against inhibitor concentration (I) at constant (S). For a competitive inhibitor of a normal enzyme, this plot is hyperbolic (Box 17-1) and eventually reaches 100% inhibition (Fig. 17-3). Furthermore, the general shape of the curve remains the same at higher values of (S), although larger amounts of inhibitor are needed to achieve 100% inhibition. The situation is quite different in the case of ATCase. Figure 17-4 shows that the maximal level of inhibition that can be achieved with CTP depends on the aspartate (substrate) concentration; higher (Asp) means lower maximal inhibition levels. This shows that CTP cannot entirely overcome the effects of

**Figure 17-3**

Competitive inhibition of a normal enzyme. Percentage of inhibition is plotted against inhibitor concentration.

**Figure 17-4**

Allosteric inhibition. Percentage of inhibition is plotted against inhibitor (CTP) concentration for various concentrations of substrate (aspartate) in the case of ATCase. [After J. C. Gerhart and A. B. Pardee, *Cold Spring Harbor Symp. Quant. Biol.* 28:491 (1963).]

#### Box 17-1 COMPETITIVE INHIBITION

To the simple mechanism of Equation 16-33, we can add the binding of a competitive inhibitor I:



We assume that the inhibitor-binding equilibrium is rapid compared to the overall reaction (Eqn. 16-33), so that the equilibrium constant  $K_1$  may be used to calculate concentrations of E and EI. It then is easy to show that, with total inhibitor concentration in great excess over total enzyme concentration, Equation 16-37 is modified to

$$v_1 = V_s / \{1 + [K_s/(S)_0][1 + (I)_0/K_1]\}$$

and the percentage of inhibition ( $I_0$ ) is given by

$$I_0 = \left(1 - \frac{V_s / \{1 + [K_s/(S)_0][1 + (I)_0/K_1]\}}{V_s / [1 + K_s/(S)_0]}\right) \times 100$$

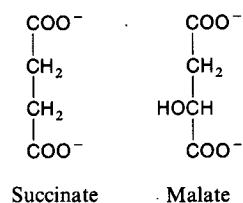
$$= \left(\frac{[K_s/(S)_0][(I)_0/K_1]}{1 + [K_s/(S)_0][1 + (I)_0/K_1]}\right) \times 100$$

Thus, at constant  $(S)_0$ , the plot of  $I_0$  versus  $(I)_0$  will be a simple hyperbolic curve.

aspartate. On the other hand, because aspartate *can* completely reverse the effects of CTP (Fig. 17-2), the situation is not symmetric with respect to the two ligands. CTP *cannot* entirely overcome the effects of aspartate, but aspartate *can* completely overcome the inhibition by CTP. This unusual interplay between CTP and aspartate sharply distinguishes this system from common competitive inhibition phenomena.

### Effect of a competitive inhibitor

The effects of a true competitive inhibitor also are unusual. Malate and succinate are structural analogs of aspartate that presumably compete with the substrate for sites on the enzyme:



However, the effect of malate, for example, varies with the aspartate concentration (Fig. 17-5). A plot of percentage of activity versus malate concentration (in the range

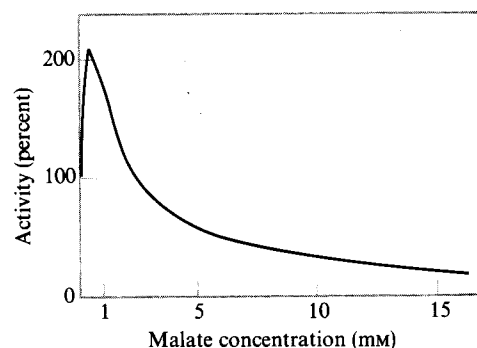


**Figure 17-5**  
Activation and inhibition of ATCase by malate.  
[After J. C. Gerhart and A. B. Pardee, *Cold Spring Harbor Symp. Quant. Biol.* 28:491 (1963).]

of low aspartate concentrations) shows high activity at low malate concentration, and progressive inhibition with higher malate concentration until activity is abolished. Thus, depending on its concentration, malate can act either as an activator or as an inhibitor. On the other hand, at much higher levels of aspartate (not shown), addition of malate leads only to inhibition, regardless of the amount of malate already present.

Allosteric proteins invariably are composed of subunits. In ATCase, there are

six catalytic (C) chains and six regulatory (R) chains. Each C chain has a molecular weight of about 33,000 d, and each R chain about 17,000 d. In the intact molecule, there are six sites for aspartate and carbamoyl phosphate on the C chains and six sites for CTP on the R chains.

Although a detailed model is not yet available, considerable progress has been made on the structure of ATCase. The work has been directed by William Lipscomb. Figure 2-49 is a schematic illustration of the structure. The enzyme has one 3-fold and three 2-fold axes. The subunits are arranged so that there is one trimer of C chains above and below a belt of three R-chain dimers. With respect to its largest dimensions, the molecule is about  $110 \times 110 \times 90 \text{ \AA}$  in size.

The reaction properties and structural features clearly show that an allosteric enzyme such as ATCase is quite different from many other enzymes. Consequently, special models have been devised to account for this kind of behavior. These models have been subjected to a number of experimental tests.

### 17-3 MONOD-WYMAN-CHANGEUX (MWC) MODEL FOR ALLOSTERIC PROTEINS

Models for allosteric proteins invariably assign an important role to the conformational states of the subunits and to subunit-subunit interactions. Because of its simplicity, a popular and frequently cited model is that of J. Monod, J. Wyman, and J.-P. Changeux (1965). Although the MWC model is not applicable to all systems, it contains concepts that are useful for discussing allosteric systems and has an unusually simple algebraic description.

The model distinguishes between protomers and subunits. A protomer is that structural unit that bears one site for each of the various ligands. A subunit is a single polypeptide chain. Therefore, a protomer may be made up of more than one subunit. In the case of ATCase, the protomer is composed of one R and one C chain.

#### Four main assumptions

The MWC model for an allosteric protein contains four essential assumptions.

1. Identical protomers occupy equivalent positions in the protein. This means the molecule must have at least one symmetry axis.
2. Each protomer contains a unique receptor site for each specific ligand.
3. At least two conformational states are reversibly accessible to the protein. In each of these states, symmetry is conserved. However, the affinity of a given ligand for the protein may be very different in the different conformational states.

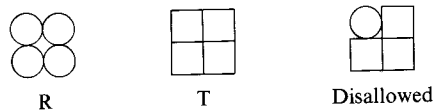
4. The binding affinity of a specific ligand depends only on the conformational state of the enzyme and not on the occupancy of neighboring sites.

### Homotropic and heterotropic interactions

The model also distinguishes between *homotropic* interactions and *heterotropic* interactions. When the binding of a ligand is influenced by how much of that same ligand is already bound, this is termed a homotropic interaction; the sigmoidal curve of velocity versus substrate concentration in Figure 17-1 is an example. When the binding of one kind of ligand to its stereospecific site affects the binding of a second kind of ligand to its stereospecific site, this is a heterotropic interaction; the effect of CTP on the curve of velocity versus aspartate concentration in Figure 17-2 is an example.

### Algebraic treatment of the MWC model

For the purpose of carrying out the algebraic development of the model, we consider a protein composed of four protomers ( $n = 4$ ). Each protomer can exist in either of two reversibly equilibrating conformational states. Following the designations of MWC, these states are denoted R (relaxed) and T (taut) forms. These are symmetrical states that we can schematically illustrate as



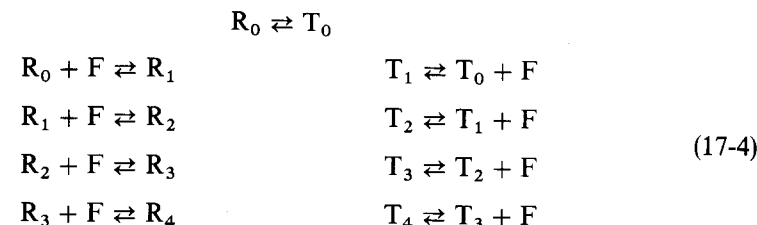
where each circle or square designates a protomer. Because it lacks symmetry (MWC assumption 3), the structure on the right and other such forms are disallowed as energetically too unfavorable.

According to assumption 4, only two microscopic dissociation constants are required to specify the binding of a ligand F to the enzyme. These microscopic constants are designated  $k_R$  and  $k_T$ , where  $k_R$  may be written, for example, as

$$k_R = \frac{\left( \begin{array}{cc} \circ & \circ \\ \circ & \circ \end{array} \right) (F)}{\left( \begin{array}{cc} \circ & \circ \\ \circ & F \end{array} \right)} = \frac{\left( \begin{array}{cc} \circ & F \\ \circ & \circ \end{array} \right) (F)}{\left( \begin{array}{cc} \circ & F \\ F & \circ \end{array} \right)} = \dots \quad (17-3)$$

Analogous expressions can be written for  $k_T$ . Ordinarily,  $k_R \neq k_T$ ; that is, the ligand preferentially binds to one form or the other (if  $k_R = k_T$ , then the two states are indistinguishable as far as F is concerned).

The binding equilibria of ligand F can be written as



In this scheme,  $R_i$  is defined as the set of all microscopic species of the R conformation that have  $i$  bound F molecules. The number of microscopic species that comprise  $R_i$  is equal to  $\Omega_{n,i}$  with  $n = 4$  (see Eqn. 15-14); for example, there are 6 microscopic species for  $i = 2$ . The same considerations apply to  $T_i$ .

In order to calculate the saturation curve of F, it is convenient to work with macroscopic equilibrium constants that are in turn proportional to the appropriate microscopic constants. These macroscopic constants are

$$k_R/4 = (R_0)(F)/(R_1) \quad (17-5a)$$

$$2k_R/3 = (R_1)(F)/(R_2) \quad (17-5b)$$

$$3k_R/2 = (R_2)(F)/(R_3) \quad (17-5c)$$

$$4k_R = (R_3)(F)/(R_4) \quad (17-5d)$$

with analogous expressions involving  $k_T$  for the T forms of the enzyme. The relationships in Equation 17-5 are easy to derive from the definition of  $k_R$  and Equation 15-14 (with  $n = 4$ ). It is convenient to express the concentration as a dimensionless parameter  $\alpha = (F)/k_R$ , so that the concentration of F is expressed in units of the microscopic dissociation constant  $k_R$ . Also, we write  $k_T = k_R/c$ , where  $c$  is a constant. (If  $c < 1$ , then F binds more strongly to the R state than to the T state.) With these parameters, we obtain the following expressions from Equation 17-5 and analogous expressions for the T species:

$$(R_1) = 4(R_0)\alpha \quad (T_1) = 4L(R_0)c\alpha \quad (17-6a)$$

$$(R_2) = 6(R_0)\alpha^2 \quad (T_2) = 6L(R_0)c^2\alpha^2 \quad (17-6b)$$

$$(R_3) = 4(R_0)\alpha^3 \quad (T_3) = 4L(R_0)c^3\alpha^3 \quad (17-6c)$$

$$(R_4) = (R_0)\alpha^4 \quad (T_4) = L(R_0)c^4\alpha^4 \quad (17-6d)$$

where  $L$  is the conformational equilibrium constant for the  $R_0 \rightleftharpoons T_0$  interconversion:<sup>8</sup>

$$L = (T_0)/(R_0) \quad (17-7)$$

The equilibrium fractional saturation  $\bar{y}_F$  with respect to F is

$$\bar{y}_F = \frac{\sum_i i(R_i) + \sum_i i(T_i)}{4[\sum_i i(R_i) + \sum_i i(T_i)]} \quad (17-8)$$

where the numerator of the right-hand side is the number of occupied sites, and the denominator is the total number of sites. The various terms in Equation 17-8 are easy to calculate:

$$\sum_{i=0}^4 (R_i) = (R_0)(1 + 4\alpha + 6\alpha^2 + 4\alpha^3 + \alpha^4) = (R_0)(1 + \alpha)^4 \quad (17-9)$$

$$\sum_{i=0}^4 (T_i) = L(R_0)(1 + c\alpha)^4 \quad (17-10)$$

$$\sum_{i=0}^4 i(R_i) = \alpha \frac{d}{d\alpha} \sum_{i=0}^4 (R_i) = 4(R_0)\alpha(1 + \alpha)^3 \quad (17-11)$$

$$\sum_{i=0}^4 i(T_i) = 4L(R_0)c\alpha(1 + c\alpha)^3 \quad (17-12)$$

Substituting these relationships into Equation 17-8, we obtain for  $\bar{y}_F$  in the case of four protomers

$$\bar{y}_F = \frac{\alpha(1 + \alpha)^3 + Lc\alpha(1 + c\alpha)^3}{(1 + \alpha)^4 + L(1 + c\alpha)^4} \quad \text{for } n = 4 \quad (17-13)$$

In general, for a protein with  $n$  protomers, we have

$$\bar{y}_F = \frac{\alpha(1 + \alpha)^{n-1} + Lc\alpha(1 + c\alpha)^{n-1}}{(1 + \alpha)^n + L(1 + c\alpha)^n} \quad (17-14)$$

<sup>8</sup> In addition to  $R_0 \rightleftharpoons T_0$ , we could have included in Equation 17-4 the conformational equilibria  $R_1 \rightleftharpoons T_1$ ,  $R_2 \rightleftharpoons T_2$ , etc. However, these are not thermodynamically independent equilibria; for example, the equilibrium ratio  $(R_2)/(T_2)$  is determined by  $k_R$ ,  $k_T$ , and  $L$  (see Eqn. 17-6). Therefore, in calculating any equilibrium property of the model, we need not consider these other conformational equilibria.

Note that, if  $L = 0$ , then<sup>12</sup>

$$\bar{y}_F = \alpha/(1 + \alpha) \quad \text{for } L = 0 \quad (17-15)$$

This is the usual expression that gives a hyperbolic saturation curve for the binding of the ligand F to identical and independent sites on a protein (cf. Eqn. 15-28).

### Behavior of $\bar{y}_F$ : effects of $L$ and $c$

It is instructive to consider the behavior of  $\bar{y}_F$  under various conditions. For example, consider the case where  $n = 4$ ,  $c = 0$ , and  $L \gg 1$ . In this case, the enzyme starts out largely in the T state, but the ligand F binds exclusively to the R state. For this case, Equation 17-13 becomes

$$\bar{y}_F = \frac{\alpha(1 + \alpha)^3}{(1 + \alpha)^4 + L} \quad \text{for } c = 0 \text{ and } L \gg 1 \quad (17-16)$$

When  $\alpha \ll 1$ , then  $\bar{y}_F \cong \alpha/L$ ; that is,  $\bar{y}_F$  increases linearly with  $\alpha$ , but with a shallow slope of  $L^{-1}$ . When  $1 \cong \alpha \ll L$ , then  $\bar{y}_F \cong \alpha/L + 3\alpha^2/L + 3\alpha^3/L + \alpha^4/L$ ; that is,  $\bar{y}_F$  begins to change rapidly in response to small changes in  $L$ . Finally, when  $\alpha \cong L$ , then  $\bar{y}_F \cong 1$ .

Figure 17-6 schematically illustrates this behavior for  $n = 4$ ,  $c = 0$ , and  $L = 10^3$ . The sigmoidal features of the curve are quite apparent. It is easy to see that, if a substrate equilibrates rapidly (relative to the rate of catalysis) with its sites on an allosteric enzyme, then the curve of velocity versus substrate concentration will be proportional to  $\bar{y}_F$ ; in such cases, the illustration (Fig. 17-6) is just as applicable to a velocity profile as to a binding curve.

In Equation 17-16, it is clear that both the initial slope, at low  $\alpha$ , and the rapidly rising part of the saturation curve are dependent on  $L$ . Figure 17-7 gives several

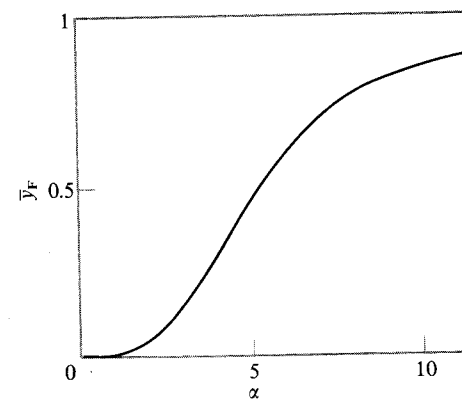
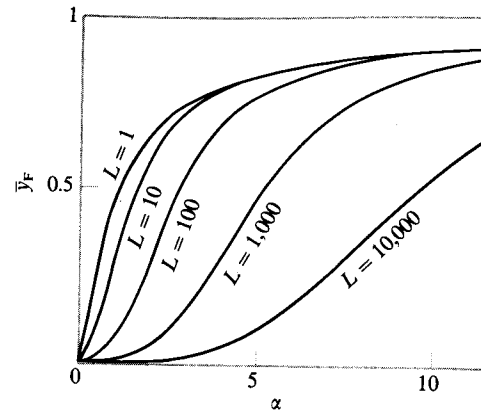


Figure 17-6

Plot of  $\bar{y}_F$  versus  $\alpha$ , for  $n = 4$ ,  $c = 0$ , and  $L = 10^3$ .



**Figure 17-7**

Effect of varying  $L$  on plot of  $\bar{y}_F$  versus  $\alpha$ , with  $c = 0$  and  $n = 4$ . [After J. Monod, J. Wyman, and J.-P. Changeux, *J. Mol. Biol.* 12:88 (1965).]

plots of  $\bar{y}_F$  versus  $\alpha$  for different values of the conformational equilibrium constant  $L$ , for the case  $c = 0$  and  $n = 4$ . It is clear that, as  $L$  increases, the sigmoidicity associated with the homotropic interactions also increases. Thus, with the ligand binding only to the R state, the greater the initial amount in the T state, the greater is the apparent cooperativity.

Figure 17-8 shows the effect on the saturation curve of varying the parameter  $c$ , with  $L = 10^3$  and  $n = 4$ . It is apparent that, as  $c$  approaches unity, the sigmoidicity of the saturation curve decreases. As implied earlier, at the limit of  $c = 1$ , the two conformational forms are indistinguishable as far as the ligand F is concerned.

In general, the greatest cooperativity is achieved when  $L$  is large and  $c$  is small (or conversely, with F preferentially binding to the T state, the greatest cooperativity occurs with small  $L$  and large  $c$ ). This behavior is a consequence of assumption 3 of the MWC model, which states that symmetry is conserved when the protein switches conformations. This means that all subunits change their conformations in a concerted fashion. Thus, when  $L$  is large, most of the protein is initially in the  $T_0$  state.

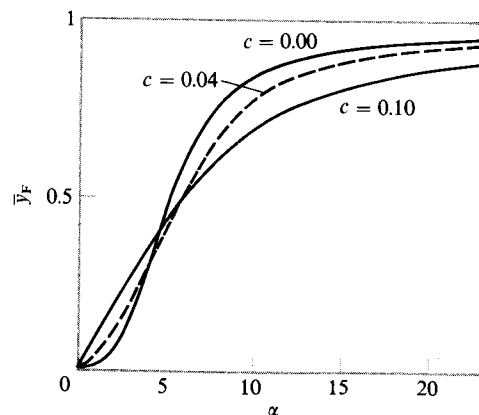


**Figure 17-8**

Effect of varying  $c$  on plot of  $\bar{y}_F$  versus  $\alpha$ , with  $L = 10^3$  and  $n = 4$ . [After J. Monod, J. Wyman, and J.-P. Changeux, *J. Mol. Biol.* 12:88 (1965).]

Binding of a ligand F (with high preference for  $R_0$ ) to give  $R_1$  pulls the overall conformational equilibria of Equation 17-4 slightly to the left, as some  $T_0$  is converted to  $R_0$  to reestablish the  $R_0 \rightleftharpoons T_0$  equilibrium. However, in the process, a disproportionately large increase in the number of available sites for F has occurred; binding of one F molecule to one site has "pulled" all  $n$  protomers (with  $n$  sites) into the R state, owing to the concerted nature of the conformational change. In this way, cooperativity results as the number of sites available to F increases many times faster than the number of molecules shifting to the R state. Of course, as more F is added, all the protein eventually shifts to the R form before it is completely saturated; at this point the binding is no longer so sensitive to the F concentration.

These ideas are best visualized by considering the behavior of the parameter  $\bar{R}$  (the fraction of molecules in the R state) as a function of (F), and by comparing the behavior of this parameter with that of  $\bar{y}_F$ .

### Comparison of the parameters $\bar{R}$ and $\bar{y}_F$

The parameter  $\bar{R}$ , the fraction of molecules in the R state, is given by

$$\bar{R} = \frac{\sum_{i=0}^n (R_i)}{\sum_{i=0}^n [(R_i) + (T_i)]} \quad (17-17)$$

$$\bar{R} = (1 + \alpha)^n / [(1 + \alpha)^n + L(1 + c\alpha)^n] \quad (17-18)$$

Equation 17-18 was obtained by substituting into Equation 17-17 the expressions for  $\sum_i (R_i)$  and  $\sum_i (T_i)$  analogous to those given in Equations 17-9 and 17-10 for the case  $n = 4$ .

As a concrete example, let  $n = 4$ ,  $c = 0$ , and  $L = 10^3$ . The expression for  $\bar{y}_F$  is given by Equation 17-16. With  $\alpha = 0$ , Equation 17-18 gives  $\bar{R} \cong L^{-1} = 0.001$ ; and  $\bar{y}_F = 0$ . Thus,  $\bar{R}$  and  $\bar{y}_F$  are essentially equal. However, when  $\alpha = 3$ , we have  $\bar{R} = 0.2$  and  $\bar{y}_F = 0.15$ ; that is,  $\bar{R}$  is now significantly larger than  $\bar{y}_F$ . This means that many molecules are in the R state but are only partially saturated with respect to F; these molecules thus have sites available to F in the conformation to which F exclusively binds (because we assumed  $c = 0$ ). Thus, when  $\alpha = 0$ , only 0.1% of the molecules (and 0.1% of the total sites) are available for F binding; this results in weak apparent binding when  $\alpha = 0$ . By the time that  $\alpha = 3$ , however, about 5% of the total sites are in the R state and are unoccupied ( $\bar{R} - \bar{y}_F$  gives the fraction of total sites that are in the R state and unoccupied). Thus, in going from  $\alpha = 0$  to  $\alpha = 1$ , there is an enormous increase in the number of unoccupied sites that are in the proper conformation for binding F. This statistical effect is responsible for the sharp, cooperative rise in the binding. As mentioned, it is a consequence of assuming that all subunits change their conformations in a concerted fashion.

Of course, as  $\alpha$  becomes increasingly large, both  $\bar{y}_F$  and  $\bar{R}$  converge to unity. The completely saturated molecule is entirely in the R state (for the example considered, where  $c = 0$ ).

### Effects of allosteric activators and inhibitors

According to the MWC model, allosteric activators and inhibitors bind preferentially to the R (activator) or T (inhibitor) state at sites distinct from the catalytic site so as to give rise to heterotropic interactions.

For simplicity, assume that an activator A binds exclusively to the R form, whereas the inhibitor I binds solely to the T form. Let the microscopic dissociation constants be  $k_{AR}$  and  $k_{IT}$ , respectively, for activator and inhibitor binding. For generality, assume that both I and A are simultaneously present. We define the parameter  $L'$  as

$$L' = \frac{\sum_{i=0}^n (T_{0,i})}{\sum_{i=0}^n (R_{0,i})} \quad (17-19)$$

where  $i$  in the numerator indexes the number of inhibitor molecules bound to the T form that has no bound F, and  $i$  in the denominator indexes the number of activator molecules bound to the R form that has no bound F. Therefore, the expressions in the numerator and denominator of Equation 17-19 are simply the total concentrations of all species that have no bound F; they formerly were designated  $(T_0)$  and  $(R_0)$ , respectively. Hence,  $L'$  is exactly analogous to  $L$ , and the two parameters are equal when  $(I) = (A) = 0$ . Proceeding by analogy with Equation 17-9, we obtain

$$\sum_{i=0}^n (R_{0,i}) = (R_{0,0})(1 + \gamma)^n \quad (17-20a)$$

$$\sum_{i=0}^n (T_{0,i}) = (T_{0,0})(1 + \beta)^n \quad (17-20b)$$

and 
$$L' = L(1 + \beta)^n / (1 + \gamma)^n \quad (17-21)$$

where  $\beta = (I)/k_{IT}$ ;  $\gamma = (A)/k_{AR}$ ; and  $L = (T_{0,0})/(R_{0,0})$  as before. The expression for  $\bar{y}_F$  can now be derived exactly as before (Eqns. 17-8 through 17-14) to give Equation 17-14 with  $L$  replaced by  $L'$ . Therefore, in the MWC model, the effects of allosteric activators and inhibitors are on the conformational equilibrium constant  $L$ .

Figure 17-9 shows the effects of  $\beta$  and  $\gamma$  on the  $\bar{y}_F$  versus  $\alpha$  plot for the case  $n = 4$ ,  $c = 0$ , and  $L = 10^3$ . It is clear that the  $\bar{y}_F$  versus (F) profile is very sensitive to (I) and (A).

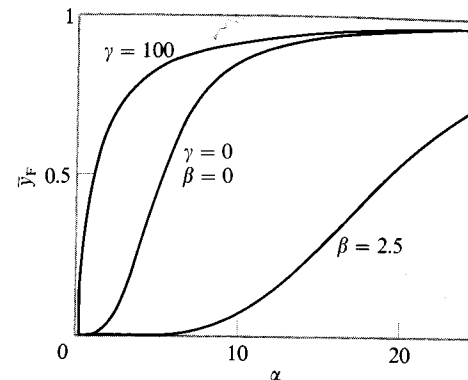


**Figure 17-9**

Effect of an allosteric activator and an inhibitor on plot of  $\bar{y}_F$  versus  $\alpha$ , with  $c = 0$ ,  $n = 4$ , and  $L = 10^3$ . [After J. Monod, J. Wyman, and J.-P. Changeux, *J. Mol. Biol.* 12:88 (1965).]

## 17-4 EXPERIMENTAL TESTS OF THE MWC MODEL

### Explanation of some data on ligand interactions

The crucial question is whether the MWC model can explain the observed data and can be critically tested by further experimentation. With ATCase, an important observation is that the allosteric inhibitor CTP cannot completely overcome the effects of the substrate aspartate, whereas aspartate can overcome the effects of CTP (Figs. 17-2 and 17-4). This observation can be explained readily by postulating that aspartate binds exclusively to the R state ( $c = 0$ ), and that CTP binds preferentially (but *not* exclusively) to the T state. Therefore, addition of sufficient aspartate will always pull the enzyme entirely into the R state. On the other hand, although CTP will produce inhibition by pulling the enzyme toward the T state, it will not cause a complete conversion to T. Because it is postulated to have some affinity for the R form, the degree to which it pulls the protein into T will be quite sensitive to the concentration of aspartate; at high concentrations of aspartate, the effects of CTP will be reduced because much of it is bound to the R form, whereas at low aspartate concentrations there will be a greater shift toward the T state in the presence of CTP. These effects can be quantitatively calculated from the model by using appropriate values for the various allosteric parameters.

Another important observation is that, at low aspartate concentrations, the competitor malate can be an activator or inhibitor (see Fig. 17-5). The model can account nicely for this behavior. Assuming that  $L$  is large, at low aspartate concentrations the enzyme is mainly in the T state. With malate, like aspartate, binding exclusively to the R form, addition of low concentrations of the competitor will promote conversion of some T to R. Moreover, the occupation of only one of  $n$  sites ( $n = 6$  for ATCase) stabilizes all  $n$  sites in the R form. As discussed, at low degrees of saturation the parameter  $\bar{R}$  substantially leads the fractional saturation. Therefore, although malate blocks a potential aspartate binding site, it also stabilizes (and shifts the conformational equilibrium toward) R forms that have *unoccupied* aspartate

sites. This accounts for the observed activation effect by malate. Of course, as the malate concentration is raised, a greater and greater proportion of the sites are bound to the competitive inhibitor so that inhibition eventually sets in.

### Relation between conformational change and fractional saturation

Although the above observations can be explained by the MWC model, a more direct test of some of the features of the model is desirable. Clearly, one of the most important assumptions is that the allosteric phenomena are a consequence of a conformational change. Related to this is the prediction that the conformational change is not colinear with the fractional saturation curve of a cooperatively binding ligand; instead, the conformational change ( $\bar{R}$ ) should lead the fractional saturation. Howard Schachman and colleagues have conducted experiments to explore this question.

An active catalytic trimer (comprised of three C chains) of ATCase can be isolated. When the catalytic trimer is titrated with the substrate analog succinate, a small systematic increase in the sedimentation coefficient  $s$  of the trimer is observed. Figure 17-10 plots the percent change in  $s$  versus the succinate concentration. It is clear that the sedimentation coefficient shifts between two plateaus as succinate is bound. This indicates that a structural alteration (change in frictional coefficient) in the catalytic trimer occurs upon binding of succinate.

Figure 17-10 also shows a "conformational" titration of the native molecule. In this case, the molecule again undergoes a shift in  $s$  between two plateaus. However, a decrease in  $s$ , rather than an increase, is observed as succinate is bound; this difference between the intact molecule and the isolated catalytic trimer might be due to

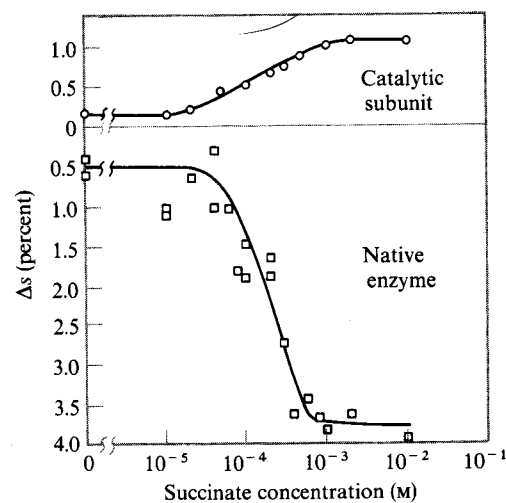
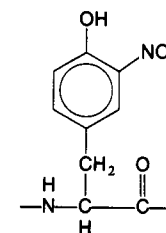


**Figure 17-10**

*Conformational titration of ATCase and the catalytic subunit. The percentage change in sedimentation coefficient is plotted against the log of the succinate concentration. [After M. W. Kirschner and H. K. Schachman, *Biochemistry* 10:1919 (1971).]*

additional changes in the intact structure beyond those that occur in the catalytic trimer. In any event, the data clearly suggest that a conformational change does occur as ligand is bound, and thus they support one feature of the model.

However, the more critical question is that of the relationship between the fractional change in conformation and the fractional saturation with respect to succinate. This question has been approached by introducing an optical probe into the C chains; the probe undergoes spectral changes in response to the binding of succinate. For this purpose, catalytic trimers were treated with tetranitromethane to give approximately one nitrotyrosine residue per C chain. This residue has an absorption maximum at 430 nm, well removed from the major absorption of the protein, which is below 300 nm. To a good approximation, the nitrated trimer catalytically behaves like the unmodified one, thus indicating that nitration does not seriously perturb the molecule.



Ordinarily, experiments are done with enough carbamoyl phosphate to saturate the protein. Binding of succinate can be followed spectrophotometrically at 430 nm. Titration of the catalytic trimer to complete saturation with succinate gives an approximately 14% decrease in absorption at 430 nm. Moreover, there is no evidence for cooperativity with the trimer. This means that cooperativity requires contributions from the quaternary structure of the intact enzyme. In addition, the fractional spectral changes due to succinate binding exactly match the fractional sedimentation changes in the catalytic trimer. This indicates that binding of succinate and the conformation change are parallel processes.

When the nitrated catalytic chains are incorporated with the R chains into the native enzyme, the resulting modified enzyme is similar in its catalytic behavior to the unmodified enzyme. Thus, in both the isolated trimer and in the intact enzyme, the introduction of the nitro group into the C chains does not produce a significant perturbation. Moreover, when the enzyme is saturated with succinate, the change in absorption per C chain at 430 nm is almost identical for the intact enzyme and for the isolated catalytic trimer.

However, the profile of the fractional spectral change versus the succinate concentration is quite different for the isolated catalytic trimer than for the intact enzyme. Figure 17-11 compares the hyperbolic binding of succinate to the trimer with the sigmoidal, cooperative binding to the intact molecule. This shows that cooperativity is a feature of the intact molecule, and requires the presence of the R chains.

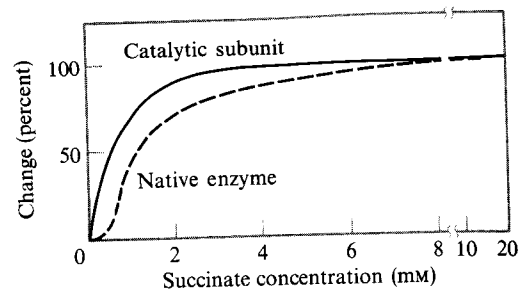


Figure 17-11

Fractional spectral change (at 430 nm) as a function of succinate concentration, for the nitrated catalytic subunit and for nitrated ATCase. [After M. W. Kirschner and H. K. Schachman, *Biochemistry* 12:2997 (1973).]

Figure 17-12 compares, for the intact enzyme, the plot of fractional spectral change versus the succinate concentration with the analogous plot of the fractional sedimentation change. It is apparent that the conformational change, as monitored by sedimentation, leads the spectral change, which monitors binding of succinate. This behavior is exactly that predicted by the MWC model.

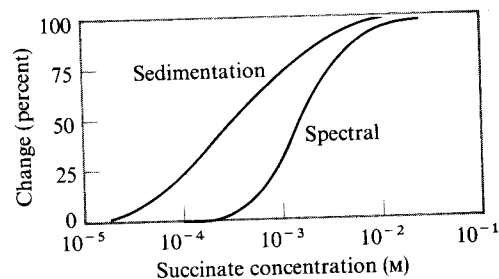


Figure 17-12

Percentage change in sedimentation and in spectrum (at 430 nm) for nitrated ATCase. [After M. W. Kirschner and H. K. Schachman, *Biochemistry* 12:2997 (1973).]

In summary, not only can some kinetic observations be explained by the model, but direct experiments demonstrate the existence of a conformational change and verify a key prediction concerning the relationship between conformational change and fractional saturation.

## 17-5 ALTERNATIVE MODELS FOR ALLOSTERIC PROTEINS

Even though many observations with ATCase and with other enzymes can be explained by the MWC model, it appears clear that the model cannot account for the behavior of all systems. Moreover, although many of the main features of ATCase are consistent with the MWC proposal, the model does not explain all observations that have been made even on this enzyme.

One of the most obvious limitations of the MWC model is its inability to accommodate *anticooperativity*. In the model, a ligand always pulls the conformational equilibrium toward the form to which it preferentially binds. This acts only to enhance

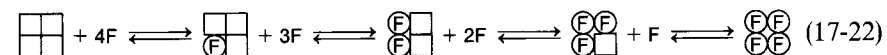
further binding of the same ligand. Under no conditions can a situation be obtained in which binding becomes substantially weaker as saturation proceeds.

Apparent anticooperativity has been observed in ligand binding, although there is some question whether true anticooperativity or other effects are responsible for the observed anticooperativity (see Gennis, 1976). Nevertheless, it is clear that, in a truly anticooperative system, an alternative to the MWC model must be used to rationalize the observations.

### A sequential model

Because of limitations in the MWC model, some data are interpreted in terms of a *sequential model*. This model has been extensively developed by D. E. Koshland and colleagues (Koshland et al., 1966). The essential idea is that ligand binding produces a sequential set of structural changes in the protein, so that a series of intermediate conformational forms are obtained. The molecule is not restricted to symmetrical conformations, so many possible conformational forms can exist. In principle, any given conformational state can assume its own unique values for the microscopic dissociation constants that characterize ligand-binding sites; as the protein binds ligand and switches from one state to another, the successive dissociation constants can increase or decrease. For this reason virtually any type of binding behavior, including anticooperativity, can be accommodated.

A simple example of a sequential scheme is



In this example, each subunit is assumed to switch from one conformational state to another as it binds ligand. Thus, the scheme in Equation 17-22 indicates that ligand binding *induces* the conformational switch in the subunit to which it binds. The conformational change may occur in part to achieve a better fit between the binding site and the ligand. When a subunit changes conformation, subunit-subunit interactions may change so that the ligand affinities of unoccupied subunits may be altered. Moreover, in an unsymmetrical intermediate such as



the total subunit-subunit interactions experienced by any given subunit can be unique for each subunit; these interactions in turn can give rise to different ligand dissociation constants for each of the unoccupied sites in an intermediate conformational form. This makes it possible to explain a wide variety of data.

## A more general scheme

Figure 17-13 shows a more general scheme for allosteric interactions. This scheme allows the individual subunits to take on freely either of two conformational forms, regardless of the number of ligands that are bound. For a four-subunit protein, this

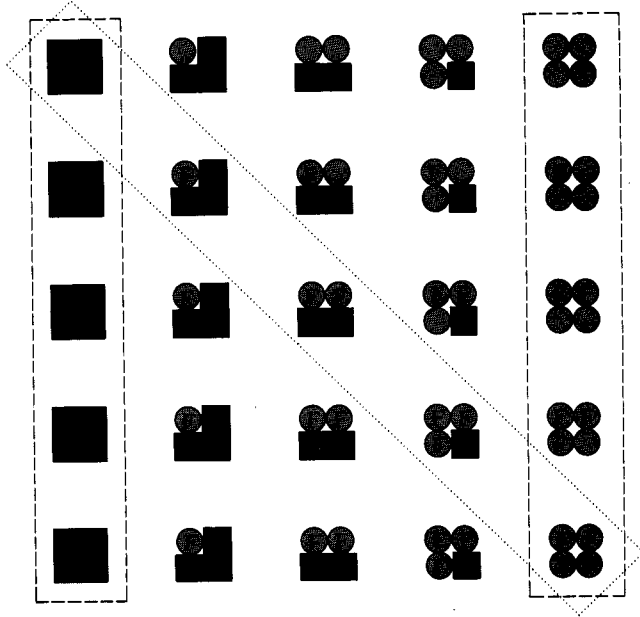


Figure 17-13

A general allosteric scheme. (See text for explanation.)  
[After G. G. Hammes and C.-W. Wu, *Science* 172:1205 (1971).]

allows 25 different forms. It is seen that the MWC model is a limiting case of this scheme, involving only the species enclosed by dashed rectangles, whereas the simple sequential scheme involves the forms enclosed by the diagonal dotted rectangle.

More complex schemes (involving more conformational forms of the subunits) than that given in Equation 17-22 or in Figure 17-13 can also be envisioned. In general, one attempts to find the simplest scheme that will accommodate all observations. For this reason, data on allosteric proteins often are interpreted in terms of the MWC model, particularly because it uses only a few parameters. However, when observations cannot be accommodated by the simple MWC framework, schemes that can accommodate more parameters, such as the simple sequential model of Equation 17-22, must be considered.

## 17-6 HEMOGLOBIN

As another example of a well-studied allosteric protein, we briefly review some of the main features of the hemoglobin system. Some aspects of hemoglobin structure and function are sketched in Chapter 2. Hemoglobin is composed of four polypeptides, two  $\alpha$  chains and two  $\beta$  chains, to give an  $\alpha_2\beta_2$  structure. The  $\alpha$  and  $\beta$  chains are structurally similar; each is about 150 amino acid residues in length and contains a single heme with an iron atom in the  $\text{Fe}^{2+}$  state. The tetrameric protein combines reversibly with four molecules of oxygen.

## Cooperative oxygen binding

Figure 17-14 compares the oxygenation curves of hemoglobin and myoglobin. The latter protein is a single polypeptide, similar to the individual hemoglobin chains and containing only one heme group. It is clear from the curves that, whereas myoglobin

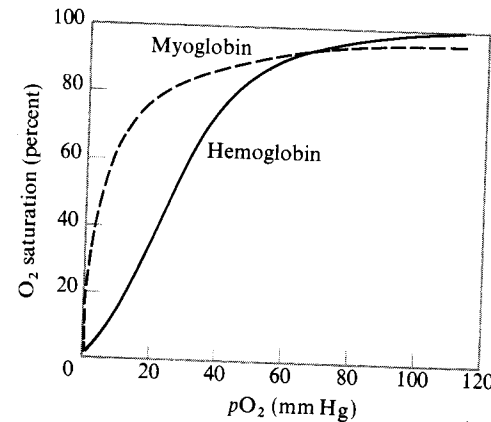


Figure 17-14

Oxygenation curves of hemoglobin and myoglobin at pH 7.4 and 38°C. [After F. Daniels and R. A. Alberty, *Physical Chemistry*, 4th ed. (New York: Wiley, 1975).]

shows the normal behavior for combination of a ligand at a single site, hemoglobin shows cooperative oxygen binding. As oxygen pressure increases, myoglobin combines with oxygen to 30% saturation before any significant association of oxygen with hemoglobin occurs. On the other hand, as a result of the steep rise in the hemoglobin curve, the two curves intersect by 90% saturation.

The steep dependence of the fractional saturation of hemoglobin on oxygen pressure has important physiological consequences. For example, it enables the molecule to respond to small changes in oxygen tension by making sizeable adjustments in the amount of oxygen released or bound.

### Treatment of oxygenation equilibrium: the Adair scheme

The oxygenation of hemoglobin can be treated by one or more of the allosteric models, such as the MWC or the sequential model or schemes that incorporate features of both. However, it is instructive to treat the problem according to a simple phenomenological scheme first used by G. S. Adair in 1925. Although the phenomenological description obscures certain of the parameters associated with a more detailed model, it has advantages for giving simple insights into the system.

The binding of oxygen may be described in terms of four macroscopic equilibria:



where  $H_i$  represents the hemoglobin species that have  $i$  bound oxygen molecules. For each stage in the reaction, we can assign a macroscopic association constant  $K_j$ , where

$$K_j = (H_{j-1})pO_2/(H_j) \quad (17-24)$$

and  $pO_2$  is the partial pressure of oxygen. The fractional saturation  $\bar{y}$  then is

$$\bar{y} = \frac{\sum_{i=0}^4 i(H_i)}{\sum_{i=0}^4 (H_i)} \quad (17-25a)$$

$$\bar{y} = \frac{\sum_{i=1}^4 \left( i(pO_2)^i \prod_{j=1}^i (1/K_j) \right)}{4 \left[ 1 + \sum_{i=1}^4 \left( (pO_2)^i \prod_{j=1}^i (1/K_j) \right) \right]} \quad (17-25b)$$

Equation 17-25b follows from Equation 17-25a through use of the equilibrium-constant relationships in Equation 17-24. The macroscopic constants  $K_j$  may be expressed in terms of microscopic constants  $k_j$ , where we define  $k_j$  as the intrinsic dissociation constant for dissociating one  $O_2$  molecule from any one of the microspecies containing  $j$  bound oxygen molecules. Thus,  $k_j$  is viewed as identical for all of the microspecies that contain  $j$  bound oxygen molecules. The relationship between  $K_j$  and  $k_j$  is given by an equation analogous to Equation 15-20:

$$K_j = (\Omega_{n,j-1}/\Omega_{n,j})k_j \quad (17-26)$$

with  $n = 4$  and  $\Omega_j$  given by Equation 15-14. For example, with  $j = 2$ , we obtain  $K_2 =$

$2k_2/3$ . Substituting Equation 17-26 into Equation 17-25b, we obtain

$$\bar{y} = \frac{(pO_2/k_1) + [3(pO_2)^2/k_1k_2] + [3(pO_2)^3/k_1k_2k_3] + [(pO_2)^4/k_1k_2k_3k_4]}{1 + (4pO_2/k_1) + [6(pO_2)^2/k_1k_2] + [4(pO_2)^3/k_1k_2k_3] + [(pO_2)^4/k_1k_2k_3k_4]} \quad (17-27)$$

### Estimates of microscopic constants for oxygen binding

Equation 17-27 may be used in conjunction with accurate measurements of  $\bar{y}$  at a large number of  $pO_2$  values in order to obtain estimates of the  $k_j$  parameters. Table 17-1 lists some experimental values of  $k_j$  obtained at 25°C in solutions buffered to pH 7.4 in the presence and absence of 0.1 M NaCl. In the absence of salt, note the progressive decrease in  $k_j$  as oxygenation proceeds; the largest change occurs between  $k_2$  and  $k_3$ . It is apparent that the last oxygen binds over 30-fold more strongly than the first one.

**Table 17-1**  
Estimated microscopic dissociation constants for human hemoglobin

	$k_1$	$k_2$	$k_3$	$k_4$
- NaCl	8.8	6.1	0.85	0.25
+ 0.1 M NaCl	42	13	12	0.14

NOTE: Values of  $k_1$  are given in units of mm Hg. These values are estimated for a solution with 10 mM Tris buffer (pH 7.4) at 25°C.

SOURCE: Data from I. Tyuma, K. Imai, and K. Shimizu, *Biochemistry* 12:1491 (1973).

If 0.1 M NaCl is added to the solution, each  $k_j$  value becomes larger, except for  $k_4$ ; the oxygenation curve is shifted to the right. As we shall see, this shift can be rationalized in terms of a stabilization of the deoxy and partial-deoxy forms of hemoglobin by anions. Note also that there is a roughly 300-fold difference between  $k_1$  and  $k_4$ . This is an enormous increase in affinity for the last oxygen versus the first one.

### Concentrations of hemoglobin species during oxygenation

The  $k_j$  values are useful for calculating concentrations of the various species  $H_j$ . Figure 17-15 plots  $H_j$  concentrations versus  $pO_2$  for the case where all  $k_j$  values are

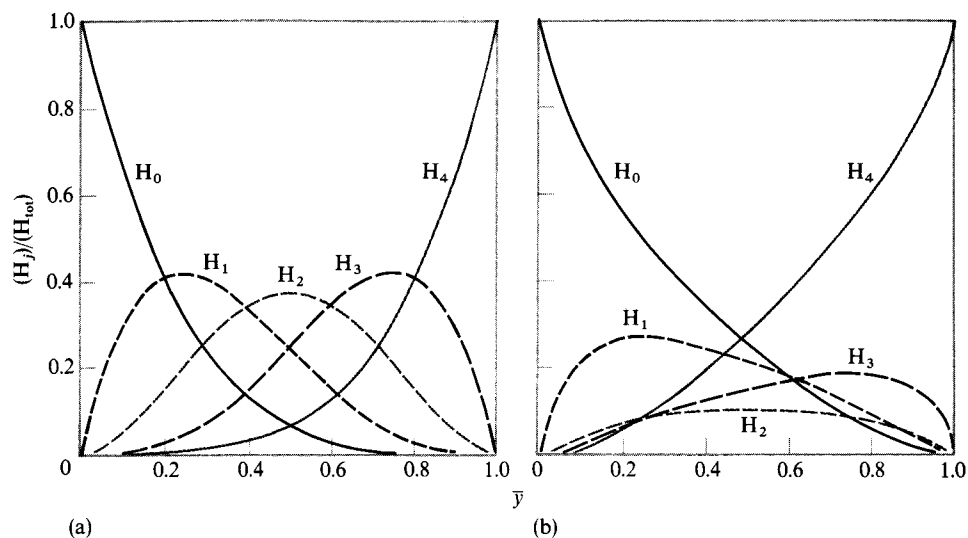


**Figure 17-15**

Fraction of hemoglobin as  $H_j$  versus  $\bar{y}$ . ( $H_{tot}$  = total hemoglobin) (a) With all  $k_j$  values equal. (b) For the  $k_j$  values (–NaCl) given in Table 17-1. [After I. Tyuma, K. Imai, and K. Shimizu, *Biochemistry* 12: 1491 (1973).]

equal (Fig. 17-15a) and for the  $k_j$  values (–NaCl) given in Table 17-1 (Fig. 17-15b). The figure illustrates the physical consequences of the cooperativity. When all  $k_j$  values are equal, each of the intermediate species  $H_1$ ,  $H_2$ , and  $H_3$  at some point during the titration rises to about 40% of the total hemoglobin concentration. In contrast, these intermediate forms are suppressed in the real situation where the value of  $k_j$  decreases with increasing  $j$ . Moreover, ( $H_4$ ) rises much sooner in Figure 17-15b than it does in Figure 17-15a; for example, when  $\bar{y} = 0.5$ , the  $H_4$  concentration represents only a few percent of the total in Figure 17-15a, but is about 30% of the total in Figure 17-15b. Thus, to a certain extent, the cooperative hemoglobin oxygenation equilibrium goes directly between the species  $H_0$  and  $H_4$ , without building up large amounts of the intermediate forms.

### The Hill constant and site–site interaction energy

It is clear from the fit of the oxygenation data to Equation 17-27 that the hemoglobin oxygenation equilibrium does not follow the simple expressions given by Equation 15-43 or 15-45. This means that the apparent Hill constant, as defined by Equation 15-46, will vary the degree of oxygenation. Figure 17-16 is a plot of  $\alpha$  versus  $pO_2$  for the case of stripped hemoglobin—that is, hemoglobin treated to remove bound organic phosphates (see below)—in low buffer concentrations. The values of  $\alpha$  were calculated from Equation 15-46. The Hill parameter rises and falls in a bell-shaped fashion as oxygenation proceeds. A value of  $\alpha = 2.5$  is obtained near the maximum,

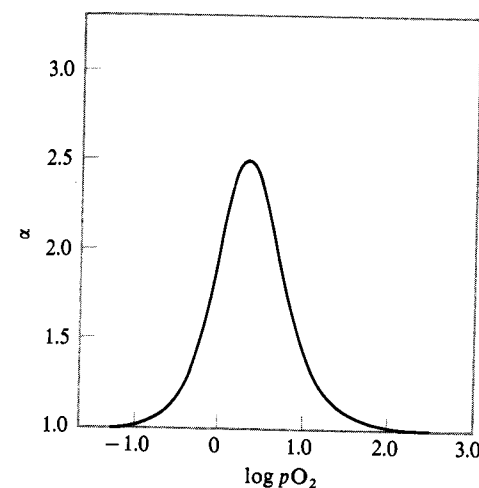


**Figure 17-16**

Plot of  $\alpha$  versus  $\log pO_2$  for stripped hemoglobin. [After I. Tyuma, K. Imai, and K. Shimizu, *Biochemistry* 12:1491 (1973).]

which occurs at about  $\bar{y} = 0.5$ . Thus, the greatest degree of apparent cooperativity occurs around the midrange of the saturation curve.

It is of interest to examine the magnitude of the interaction energy between sites  $i$  and  $j$  that gives rise to the cooperative binding. We did just this in Chapter 15 (following the discussion of Eqn. 15-39) for the case  $i = 1$  and  $j = 4$ . (With these values of  $i$  and  $j$ , we actually are comparing the affinity of a vacant site when all other sites are occupied versus that when all other sites are vacant.) Using data in Table 17-1, we calculate the value of the interaction energy  $\Delta G_{1,ij}$  to be  $-2.1 \text{ kcal mole}^{-1} \text{ site}^{-1}$  in the absence of NaCl. Thus, for the whole molecule with four sites, the total interaction energy is about  $-8.4 \text{ kcal mole}^{-1}$  ( $25^\circ\text{C}$ ).

### Bohr effect

The association of oxygen with hemoglobin is strongly dependent on pH. Figure 17-17 plots the oxygen saturation (in percent) versus  $pO_2$  at three different pH values. As pH

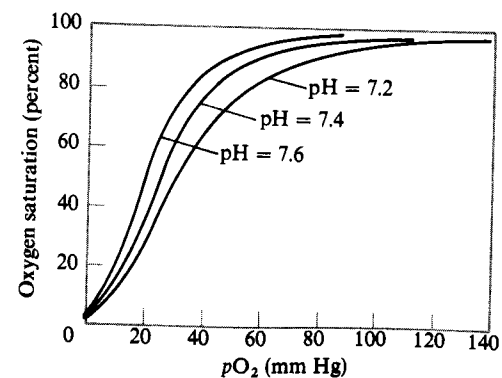


**Figure 17-17**

The Bohr effect: the effect of pH on the oxygenation curve of hemoglobin. [After R. E. Benesch and R. Benesch, *Adv. Protein Chem.* 28:211 (1974).]